A Simple 18-Pulse Star Rectifier Using Two Passive Auxiliary Circuits at DC Link

Md. Abdul Malek, *Graduate Student Member, IEEE*, and Muhammad Abdul Goffar Khan, *Senior Member, IEEE*

***Abstract*—In this article, a simple 18-pulse star rectifier using two new passive auxiliary circuits at dc link is proposed for reducing the harmonics content in ac line current. The proposed rectifier combines a double-star rectifier and four-tapped interphase reactor (FTIPR) with four diodes. Passive auxiliary circuits increase the state of the output voltage and current of the double-star rectifier, thereby increasing the pulse number of the load voltage and step number of the input line current. When FTIPR is optimally designed, passive auxiliary circuits convert double-star rectifier to 18-pulse star rectifier. Tap ratios of the FTIPR are determined based on minimum total harmonic distortion (THD) of the input line current and minimum ripple of the output voltage. The proposed rectifier simultaneously reduces ripple of the output voltage and THD of the input line current. A prototype is developed to verify the theoretical analysis through experimental results. Theoretical THD of the input line current is about 10.1%, whereas experimental THD is about 5.44%.**

***Index Terms*—18-pulse star rectifier, interphase reactor (IPR), passive auxiliary circuit, tap ratio, total harmonic distortion (THD).**

I. Introduction

THE demand of direct current (dc) is rapidly increasing in the industry. But the electrical utility generates alternating current (ac) and distributes to the consumer at fixed frequency. Therefore, diode rectifier is widely used in industrial application for converting ac power to dc power [1]. However, the traditional three-phase star and bridge rectifier distort the input line current by injecting harmonics and THD of the input line current fails to satisfy the requirement of the IEEE-519 standard [2]. Therefore, several methods are proposed for diode rectifier to decrease harmonics injection in the input line current [3]–[14]. Among them, multipulse rectifier is an efficient approach for reducing THD of the input line current [3]–[7]. Main designing goal of the multipulse rectifier is to obtain higher pulse number because harmonics reduction capability depends on pulse number. But higher pulse number makes the phase-shifting transformer more complicated and requires more number of diode.

Manuscript received July 15, 2021; revised October 8, 2021; accepted November 10, 2021. Date of publication November 19, 2021; date of current version January 19, 2022. This work was supported by the Research and Extension of RUET under Project DRE/7/RUET/489(31)/PRO/2020-21/05. Recommended for publication by Associate Editor M. Harfman Todorovic. *(Corresponding author: Md. Abdul Malek.)*

The authors are with the Department of Electrical & Electronic Engineering, Rajshahi University of Engineering & Technology, Rajshahi 6204, Bangladesh (e-mail: m.a.malekb88@gmail.com; agmagk@gmail.com).

Color versions of one or more figures in this article are available at https://doi.org/10.1109/TPEL.2021.3129262.

Digital Object Identifier 10.1109/TPEL.2021.3129262

Among the multipulse star rectifiers [4]–[7], double-star rectifier is widely used due to high reliability and simple constriction of the transformer. But input line current THD of the double-star rectifier is about 31%, which is much higher than the acceptable level specified by the IEEE-519 standard. Therefore, active injection method at dc-link is proposed for the double-star rectifier to reduce THD of the input line current [8]. Active injection method generates harmonics current through controlling the semiconductor switches of the active injection circuit and then generated harmonics current is injected to the load. It eliminates harmonics from the input line current when generated harmonics current satisfies the several conditions. However, active injection method does not reduce ripple of the output voltage, requires complex control circuit, and unable to decrease the harmonics when one switch of the active circuit is broken down.

Installing passive auxiliary circuit at dc-link of the rectifier is an interesting method to increase the amount of pulse of the rectifier without any modification of the phase-shifting transformer [9]–[13]. Passive auxiliary circuit simultaneously improves the power quality at the output side and input side of the rectifier. Dual-tapped interphase reactor (DTIPR)-based passive auxiliary circuit can double the pulse number of the output voltage of the double-star rectifier by turning ON the two diodes on the tapped alternately which effectively reduces THD of the input line current [9]. However, input line current THD of 12-pulse rectifier is much higher than the acceptable level specified by the IEEE-519 standard, and DTIPR-based passive auxiliary circuit is connected series with the load which increases conduction loss. In [10], interphase reactor (IPR) with secondary winding (IPRSW)-based passive auxiliary circuit is proposed, which converts double-star rectifier to 12-pulse star rectifier. IPRSW-based passive auxiliary circuit generates rectangular current which is circulated through the load to increases the state of the output voltage and output current of each star rectifier, and then multiplies the number of pulses of the double-star rectifier by twice. However, IPRSW-based passive auxiliary circuit requires extra secondary winding in the IPR and its harmonics reduction ability is limited. Tapped interphase reactor with secondary winding (TIPRSW)-based passive axillary circuit can multiply the pulse number of the rectifier by three times [12], [13]. However, TIPRSW-based passive auxiliary circuit requires extra secondary winding in the IPR, which increases system complexity as well as the kilovolt-ampere (KVA) rating of the IPR. Triple-tapped interphase reactor (TTIPR)-based auxiliary circuit requires two MOSFETs and three diodes to multiply the pulse number of the rectifier by three times [14]. However,

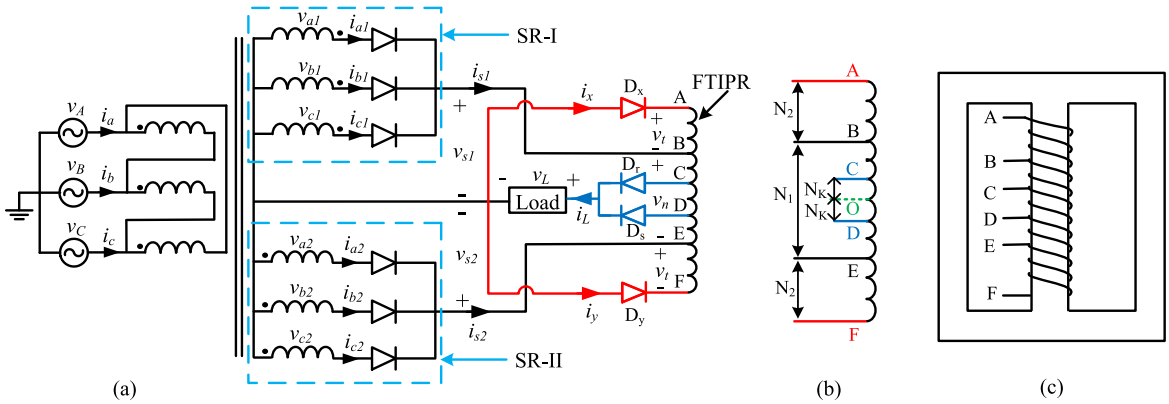

Fig. 1. (a) Proposed 18-pulse star rectifier. (b) Tap structure of FTIPR. (c) Winding configuration of FTIPR.

TTIPR-based auxiliary circuit requires complicated control circuit to turn ON the MOSFETs.

The aim of this article is to improve the harmonics rejection ability of the double-star diode rectifier by designing two new passive auxiliary circuits at dc link. The proposed passive auxiliary circuits increase the pulse number of the output voltage and step number of the input line current of the double-star rectifier by three times. Four-tapped interphase reactor (FTIPR) of the passive auxiliary circuits has four tap points but passive auxiliary circuits do not require any control circuit and thyristor/MOSFETs. Tapped points of the FTIPR are designed optimally in order to convert double-star rectifier to 18-pulse star rectifier. THD of the input line current is obtained about 5.44% in the experiment, which is lower than the theoretical value of 10.1% due to leakage inductance of the transformer. The proposed rectifier does not require phase-shifting transformer, active device, and secondary winding of the FTIPR, thereby making it simple, passive, inexpensive, and robust.

II. Circuit Configuration

Fig. 1(a) shows the circuit configuration of the proposed 18-pulse star rectifier. It consists of two star rectifiers, delta/star/star transformer with two passive auxiliary circuits. Output terminals of star rectifier-I (SR-I) and star rectifier-II (SR-II) are connected to B and E taps of the FTIPR, respectively. Diodes D_r and D_s are connected to C and D taps of the FTIPR, respectively, which is named first passive auxiliary circuit (FPAC). It is connected in series with the load. Second passive auxiliary circuit (SPAC) is constituted by connecting the diodes D_x and D_y in A and F terminals of the FTIPR, respectively. FPAC increases the output currents state of the SR-I and SR-II, which converts double-star rectifier to asymmetrical 12-pulse star rectifier without SPAC. SPAC further increases the output currents and output voltages state of the SR-I and SR-II by injecting rectangular current to the load, and then upgrades asymmetrical 12-pulse star rectifier to 18-pulse star rectifier.

Tap structure and winding configuration of the FTIPR are shown in Fig. 1(b) and (c), respectively. FTIPR has four taps on its winding, which is denoted as B, C, D, and E. O is the center point of the FTIPR; N_k is the number of turn of the winding OC and OD; N_1 is the number of turn of the winding BE; and N_2 is the number of turn of the winding AB and EF. Tap ratios k and x of the FTIPR are defined as

$$k = \frac{N_k}{N_1} \tag{1}$$

$$x = \frac{N_2}{N_1}. \tag{2}$$

III. Operation Mode

Operation of the proposed 18-pulse star rectifier depends on the relation among the voltages across the windings of the FTIPR and output voltage. Voltages across the windings AB, BE, and EF are denoted as v_t, v_n, and v_t, respectively, and output voltage of the proposed rectifier is denoted as v_L. According to the relation among v_n, v_L, and v_t, the proposed rectifier has four operation modes. Four operation modes are explained as follows.

R-Mode: Whenever $v_n > 0$ and $v_t+(k+0.5)v_n<v_L$, the proposed rectifier operates under R-mode, which is shown in Fig. 2(a). In this mode, diode D_r of the FPAC is forward biased and ON-state, and other diode D_s is reverse-biased and OFF-state. SR-I and SR-II both work, and SR-I output current i_{s1} and SR-II output current i_{s2} flow through diode D_r to supply the load. Diodes D_x and D_y of the SPAC are reverse-biased and OFF-state, the currents i_x and i_y are zero, and SPAC does not work. Assume the output current i_L is constant and considered as I_L. The current relationship in this mode is expressed as

$$\begin{cases} i_x = 0 \\ i_y = 0 \end{cases} \tag{3}$$

$$I_L = i_{s1} + i_{s2}. \tag{4}$$

The magnetomotive force (MMF) relation of the FTIPR is expressed as

$$i_{s1}(0.5N_1 - kN_1) = i_{s2}(0.5N_1 + kN_1). \tag{5}$$

From (4) and (5), the currents i_{s1} and i_{s2} are determined as

$$\begin{cases} i_{s1} = (0.5 + k)I_L \\ i_{s2} = (0.5 - k)I_L. \end{cases} \tag{6}$$

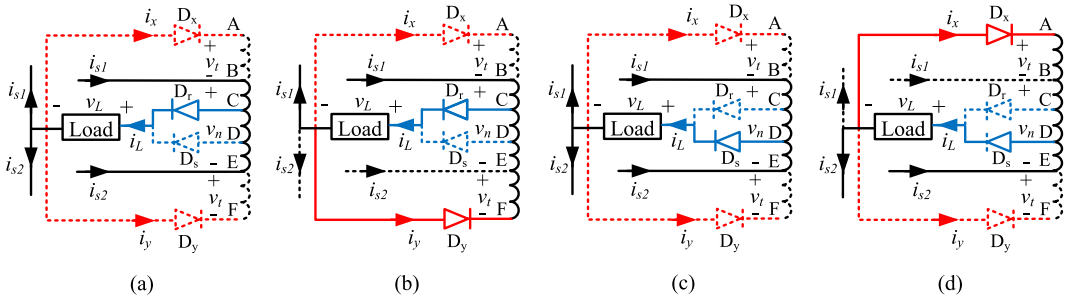

Fig. 2. Operation mode. (a) R-mode. (b) Y-mode. (c) S-mode. (d) X-mode.

The relations among SR-I output voltage v_{s1}, SR-II output voltage v_{s2}, output voltage v_L, and voltage v_n are determined as

$$v_L = v_{s1} - (0.5 - k)v_n \tag{7}$$

$$v_L = v_{s2} + (0.5 + k)v_n \tag{8}$$

$$v_n = v_{s1} - v_{s2}. \tag{9}$$

Y-Mode: Whenever $v_n > 0$ and $v_t + (k+0.5)v_n > v_L$, the proposed rectifier operates under Y-mode, which is shown in Fig. 2(b). In this mode, diode D_r of the FPAC is forward-biased and ON-state, and other diode D_s is reverse-biased and OFF-state. Diode D_x of the SPAC is reverse-biased and OFF-state, other diode D_y is forward-biased and ON-state, and rectangular-shaped current i_y is injected to the load through the diodes D_r and D_y. SR-II is reverse-biased because cathode terminal voltage v_t of the diodes of SR-II is higher than the anode terminal voltages (v_{a2}, v_{b2}, and v_{c2}). SR-I conducts and its output current i_{s1} flows through diode D_r to supply the load. The current relationship in this mode is expressed as

$$\begin{cases} i_{s2} = 0 \\ i_x = 0 \end{cases} \tag{10}$$

$$I_L = i_{s1} + i_y. \tag{11}$$

The MMF relation of the FTIPR is expressed as

$$i_{s1}(0.5N_1 - kN_1) = i_y(N_2 + 0.5N_1 + kN_1). \tag{12}$$

From (11) and (12), currents i_{s1} and i_y are determined as

$$i_{s1} = \frac{k + x + 0.5}{x + 1} I_L \tag{13}$$

$$i_y = \frac{0.5 - k}{x + 1} I_L. \tag{14}$$

The relations among v_{s1}, v_{s2}, v_L, and v_n are determined as

$$v_L = \frac{k + x + 0.5}{x + 1} v_{s1} \tag{15}$$

$$v_{s2} = \frac{x}{x + 1} v_{s1} \tag{16}$$

$$v_n = \frac{1}{x + 1} v_{s1}. \tag{17}$$

S-Mode: Whenever $v_n < 0$ and $-v_t - (k+0.5)v_n < v_L$, the proposed rectifier operates under S-mode, which is shown in Fig. 2(c). In this mode, diode D_r of the FPAC is reverse-biased and OFF-state, and other diode D_s is forward-biased and ON-state. SR-I and SR-II both work, and SR-I output current i_{s1} and SR-II output current i_{s2} flow through diode D_s to supply the load. Diodes D_x and D_y of the SPAC are reverse-biased and OFF-state, currents i_x and i_y are zero, and SPAC does not work. The current relationship in this mode is expressed as

$$I_L = i_{s1} + i_{s2} \tag{18}$$

$$\begin{cases} i_x = 0 \\ i_y = 0. \end{cases} \tag{19}$$

The MMF relation of the FTIPR is expressed as

$$i_{s1}(0.5N_1 + kN_1) = i_{s2}(0.5N_1 - kN_1). \tag{20}$$

From (18) and (20), currents i_{s1} and i_{s2} are determined as

$$\begin{cases} i_{s1} = (0.5 - k)I_L \\ i_{s2} = (0.5 + k)I_L. \end{cases} \tag{21}$$

The relations among v_{s1}, v_{s2}, v_L, and v_n are determined as

$$v_L = v_{s1} - (0.5 + k)v_n \tag{22}$$

$$v_L = v_{s2} + (0.5 - k)v_n \tag{23}$$

$$v_n = v_{s1} - v_{s2}. \tag{24}$$

X-Mode: Whenever $v_n < 0$ and $-v_t - (k + 0.5)v_n > v_L$, the proposed rectifier operates under X-mode, which is shown in Fig. 2(d). In this mode, diode D_r of the FPAC is reverse-biased and OFF-state, and other diode D_s is forward-biased and ON-state. Diode D_x of the SPAC is forward-biased and ON-state, and other diode D_y is reverse-biased and OFF-state, and rectangular-shaped current i_x is injected to the load through diodes D_s and D_x. SR-I is reverse-biased because cathode terminal voltage $-v_t$ of the diodes of the SR-I is higher than the anode terminal voltages (v_{a1}, v_{b1}, and v_{c1}). SR-II conducts and its output current i_{s2} flows through diode D_S to supply the load. The current relationship in this mode is expressed as

$$\begin{cases} i_{s1} = 0 \\ i_y = 0 \end{cases} \tag{25}$$

$$I_L = i_{s2} + i_x. \tag{26}$$

The MMF relation of the FTIPR is expressed as

$$i_{s2}(0.5N_1 - kN_1) = i_x(N_2 + 0.5N_1 + kN_1). \tag{27}$$

From (26) and (27), the currents i_{s2} and i_x are determined as

$$i_{s2} = \frac{k + x + 0.5}{x + 1} I_L \tag{28}$$

$$i_x = \frac{0.5 - k}{x + 1} I_L. \tag{29}$$

The relations among v_{s1}, v_{s2}, v_L, and v_n are determined as

$$v_L = \frac{k + x + 0.5}{x + 1} v_{s2} \tag{30}$$

$$v_{s1} = \frac{x}{x + 1} v_{s2} \tag{31}$$

$$v_n = -\frac{1}{x + 1} v_{s2}. \tag{32}$$

Fig. 3 shows the waveforms of different parts of the proposed rectifier under optimum tap ratios. Voltages v_n and v_t of the FTIPR are shown in Fig. 3(a) and (b), respectively. Current through diodes D_r and D_s of the FPAC are denoted as i_r and i_s, which are shown in Fig. 3(c) and (d), respectively. Rectangular-shaped current i_y and i_x of the SPAC are shown in Fig. 3(e) and (f), respectively. As shown in Fig. 3(c)–(f), diodes D_r, D_s, D_y, and D_x of the passive auxiliary circuits are turned ON three times per cycle. Fig. 3(g) and (h) show the output currents of the SR-1 and SR-II, respectively. As shown in Fig. 3(g) and (h), FPAC and SPAC increase the state of the output currents of SR-1 and SR-2, thereby increasing the step in the input line current to 18 numbers. Fig. 3(k) shows the input line current which contains 18 steps per cycle. FPAC and SPAC also increase the state of the output voltages of SR-I and SR-II, which are shown in Fig. 3(i) and (j), respectively. The changes in the voltages of the SR-I and SR-II increase the pulse number of the output voltage of the proposed rectifier from 6 to 18, which is shown in Fig. 3(l).

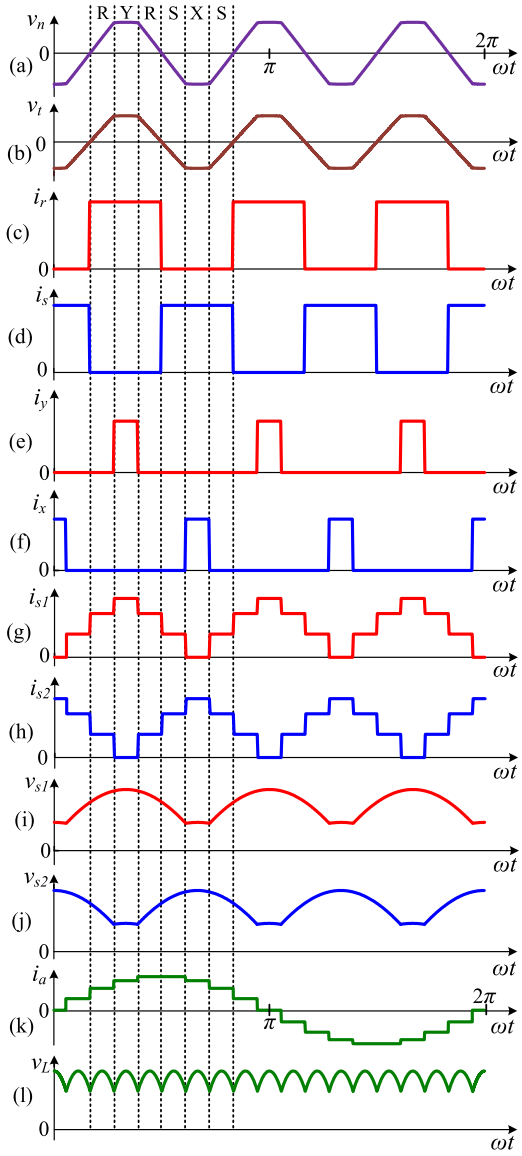

Fig. 3. (a) Voltage v_n of FTIPR. (b) Voltage v_t of FTIPR. (c) Current i_r through diode D_r of FPAC. (d) Current i_s through diode D_s of FPAC. (e) Current i_y through diode D_y of SPAC. (f) Current i_x through diode D_x of SPAC. (g) Output current i_{s1} of SR-I. (h) Output current i_{s2} of SR-II. (i) Output voltage v_{s1} of SR-I. (j) Output voltage v_{s2} of SR-II. (k) Input line current i_a. (l) Output voltage v_L of the proposed 18-pulse star rectifier.

IV. Optimum Tap Ratio of FTIPR

The analysis of operation mode shows that the output currents of SR-I and SR-II are function of the tap ratios of the FTIPR, which indicate input line current also function of the tap ratios. Output voltage of the proposed rectifier also depends on the tap ratios. Therefore, tap ratios affect THD of the input line current and ripple of the output voltage. In this section, optimum tap ratios are determined from the view of minimum THD of the input line current and ripple of the output voltage.

A. Optimum Tap Ratio Based on Minimum THD of Input Line Current

The relation between input line currents and tap ratios is established in this section for finding the optimal tap ratios from the viewpoint of minimum input line current THD. Therefore, switching functions S_{a1}, S_{b1}, S_{c1}, S_{a2}, S_{b2}, and S_{c2} are introduced for establishing the relation between ac-side input line currents and dc-side currents. S_{a1} is expressed as

$$S_{a1} = \begin{cases} 1, & \text{for } 0 \le \omega t \le \frac{2\pi}{3} \\ 0, & \text{for } \frac{2\pi}{3} \le \omega t \le 2\pi. \end{cases} \tag{33}$$

Other switching functions S_{b1}, S_{c1}, S_{a2}, S_{b2}, and S_{c2} can be determined by shifting S_{a1} with $-120°$, $-240°$, $-180°$, $60°$, $-60°$, respectively. The relation between input side currents and output side currents of the SR-I and SR-II can be expressed as

$$\begin{bmatrix} i_{a1} \\ i_{b1} \\ i_{c1} \end{bmatrix} = \begin{bmatrix} S_{a1} \\ S_{b1} \\ S_{c1} \end{bmatrix} i_{s1} \tag{34}$$

$$\begin{bmatrix} i_{a2} \\ i_{b2} \\ i_{c2} \end{bmatrix} = \begin{bmatrix} S_{a2} \\ S_{b2} \\ S_{c2} \end{bmatrix} i_{s2}. \tag{35}$$

For the simplicity of analysis, assume turn ratio of the delta/star/star transformer is one. According to the Kirchhoff's current law, the input line currents of the proposed rectifier can be determined as

$$\begin{bmatrix} i_a \\ i_b \\ i_c \end{bmatrix} = \begin{bmatrix} S_{a1} - S_{c1} & S_{c2} - S_{a2} \\ S_{b1} - S_{a1} & S_{a2} - S_{b2} \\ S_{c1} - S_{b1} & S_{b2} - S_{c2} \end{bmatrix} \begin{bmatrix} i_{s1} \\ i_{s2} \end{bmatrix}. \tag{36}$$

The expressions of currents i_{s1} and i_{s2} can be determined from the analysis of operation mode and expressed as

$$i_{s1} = \begin{cases} 0 & \omega t \in [0 + \frac{2n\pi}{3}, \beta + \frac{2n\pi}{3}] \\ (0.5-k)I_L & \omega t \in [\beta + \frac{2n\pi}{3}, \frac{\pi}{6} + \frac{2n\pi}{3}] \\ (0.5+k)I_L & \omega t \in [\frac{\pi}{6} + \frac{2n\pi}{3}, \frac{\pi}{3} - \beta + \frac{2n\pi}{3}] \\ \frac{k+x+0.5}{x+1} I_L & \omega t \in [\frac{\pi}{3} - \beta + \frac{2n\pi}{3}, \frac{\pi}{3} + \beta + \frac{2n\pi}{3}] \\ (0.5+k)I_L & \omega t \in [\frac{\pi}{3} + \beta + \frac{2n\pi}{3}, \frac{\pi}{2} + \frac{2n\pi}{3}] \\ (0.5-k)I_L & \omega t \in [\frac{\pi}{2} + \frac{2n\pi}{3}, \frac{2\pi}{3} - \beta + \frac{2n\pi}{3}] \\ 0 & \omega t \in [\frac{2\pi}{3} - \beta + \frac{2n\pi}{3}, \frac{2\pi}{3} + \frac{2n\pi}{3}] \end{cases} \tag{37}$$

$$i_{s2} = \begin{cases} \frac{k+x+0.5}{x+1} I_L & \omega t \in [0 + \frac{2n\pi}{3}, \beta + \frac{2n\pi}{3}] \\ (0.5+k)I_L & \omega t \in [\beta + \frac{2n\pi}{3}, \frac{\pi}{6} + \frac{2n\pi}{3}] \\ (0.5-k)I_L & \omega t \in [\frac{\pi}{6} + \frac{2n\pi}{3}, \frac{\pi}{3} - \beta + \frac{2n\pi}{3}] \\ 0 & \omega t \in [\frac{\pi}{3} - \beta + \frac{2n\pi}{3}, \frac{\pi}{3} + \beta + \frac{2n\pi}{3}] \\ (0.5-k)I_L & \omega t \in [\frac{\pi}{3} + \beta + \frac{2n\pi}{3}, \frac{\pi}{2} + \frac{2n\pi}{3}] \\ (0.5+k)I_L & \omega t \in [\frac{\pi}{2} + \frac{2n\pi}{3}, \frac{2\pi}{3} - \beta + \frac{2n\pi}{3}] \\ \frac{k+x+0.5}{x+1} I_L & \omega t \in [\frac{2\pi}{3} - \beta + \frac{2n\pi}{3}, \frac{2\pi}{3} + \frac{2n\pi}{3}] \end{cases} \tag{38}$$

where $n = 0, 1, 2, 3, 4, \ldots$.

The input line current i_a can be determined by substituting (37) and (38) into (36) and expressed as

$$i_a = \begin{cases} 0 & \omega t \in [0, \beta] \\ (0.5-k)I_L & \omega t \in [\beta, \frac{\pi}{6}] \\ (0.5+k)I_L & \omega t \in [\frac{\pi}{6}, \frac{\pi}{3} - \beta] \\ \frac{k+x+0.5}{x+1} I_L & \omega t \in [\frac{\pi}{3} - \beta, \frac{\pi}{3} + \beta] \\ I_L & \omega t \in [\frac{\pi}{3} + \beta, \frac{\pi}{2}] \end{cases} \tag{39}$$

where β is the initial conduction angle. Initial conduction angle β is determined as

$$\beta = \left[\tan^{-1}\left\{\frac{2}{\sqrt{3}}(x+0.5)\right\}\right] - \frac{\pi}{3}. \tag{40}$$

From (39), the rms value of the input line current is determined as

$$I_a = I_L \times \sqrt{\frac{2}{\pi}\left[(1.5+2k^2)\left(\frac{\pi}{6} - \beta\right) + \frac{2(k+x+0.5)^2}{(x+1)^2}\beta\right]}. \tag{41}$$

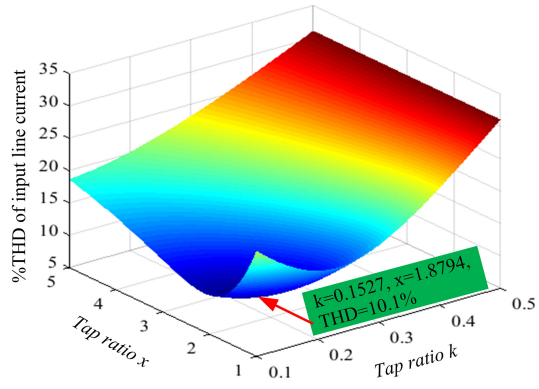

Fig. 4. Relation among THD, x, and k.

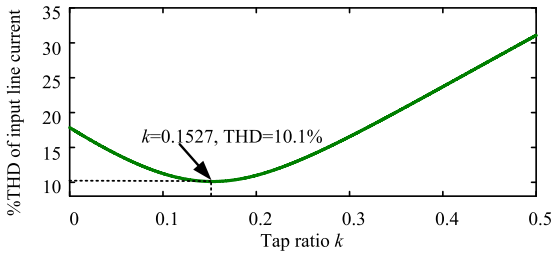

Fig. 5. Relation between THD and tap ratio k when $x = 1.8794$.

The rms value of fundamental component of the input line current is determined as

$$I_{1a} = \frac{2\sqrt{6}I_L}{\pi}\left[k + \frac{\sqrt{3}}{4}(1-2k)\cos\beta + A_1 \sin\beta\right] \tag{42}$$

where $A_1 = (\frac{k+x+0.5}{x+1} - \frac{2k+3}{x+1})$.

THD of the input line current is defined as

$$\%\text{THD} = \frac{\sqrt{I_a^2 - I_{1a}^2}}{I_{1a}}. \tag{43}$$

THD of the input line current is calculated by substituting (41) and (42) into (43). Optimum tap ratios are obtained by minimizing the THD of the input line current. The relation among tap ratios k, x, and THD is shown in Fig. 4. It is seen from Fig. 4 that THD of the input line current is minimum when $k = 0.1527$ and $x = 1.8794$. Hence, optimum values of tap ratios k and x are 0.1527 and 1.8794, respectively, and under these optimum values, THD of the input line current is about 10.1%. When $x = 1.8794$, the relation between THD and tap ratio k is shown in Fig. 5. When $k = 0.1527$, the relation between THD and tap ratio x is shown in Fig. 6.

B. Optimum Tap Ratio Based on Minimum Ripple Factor of Output Voltage

The relation between output voltage and tap ratios is established in this section for finding the optimum tap ratios from the viewpoint of minimum output voltage ripple factor.

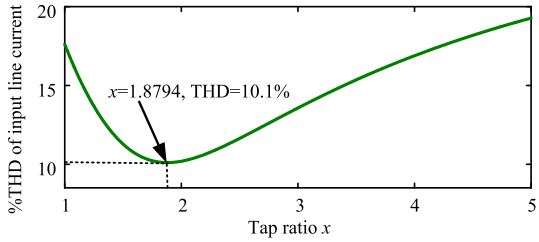

Fig. 6. Relation between THD and tap ratio x when $k = 0.1527$.

Expressions of the voltages v_{s1}, v_{s2}, and v_n can be determined from the analysis of operation mode and expressed as

$$v_{s1} = \begin{cases} \frac{x}{x+1}\sqrt{3}V_m \sin\left(\omega t + \frac{\pi}{2}\right) & \omega t \in [0, \beta] \\ \sqrt{3}V_m \sin\left(\omega t + \frac{\pi}{6}\right) & \omega t \in [\beta, \frac{2\pi}{3} - \beta] \\ \frac{x}{x+1}\sqrt{3}V_m \sin\left(\omega t - \frac{\pi}{6}\right) & \omega t \in [\frac{2\pi}{3} - \beta, \frac{2\pi}{3}] \end{cases} \tag{44}$$

$$v_{s2} = \begin{cases} \sqrt{3}V_m \sin\left(\omega t + \frac{\pi}{2}\right) & \omega t \in [0, \frac{\pi}{3} - \beta] \\ \frac{x}{x+1}\sqrt{3}V_m \sin\left(\omega t + \frac{\pi}{6}\right) & \omega t \in [\frac{\pi}{3} - \beta, \frac{\pi}{3} + \beta] \\ \sqrt{3}V_m \sin\left(\omega t - \frac{\pi}{6}\right) & \omega t \in [\frac{\pi}{3} + \beta, \frac{2\pi}{3}] \end{cases} \tag{45}$$

$$v_n = \begin{cases} -\frac{1}{x+1}\sqrt{3}V_m \sin\left(\omega t + \frac{\pi}{2}\right) & \omega t \in [0, \beta] \\ -\sqrt{3}V_m \cos\left(\omega t + \frac{\pi}{3}\right) & \omega t \in [\beta, \frac{\pi}{3} - \beta] \\ \frac{1}{x+1}\sqrt{3}V_m \sin\left(\omega t + \frac{\pi}{6}\right) & \omega t \in [\frac{\pi}{3} - \beta, \frac{\pi}{3} + \beta] \\ \sqrt{3}V_m \cos\left(\omega t\right) & \omega t \in [\frac{\pi}{3} + \beta, \frac{2\pi}{3} - \beta] \\ -\frac{1}{x+1}\sqrt{3}V_m \sin\left(\omega t - \frac{\pi}{6}\right) & \omega t \in [\frac{2\pi}{3} - \beta, \frac{2\pi}{3}] \end{cases} \tag{46}$$

where V_m is the amplitude of the input phase voltage.

According to the relationship among v_{s1}, v_{s2}, v_n, and v_L, the output voltage is determined as

$$v_L = \sqrt{3}V_m \times \begin{cases} \frac{k+x+0.5}{x+1}\sin\left(\omega t + \frac{\pi}{2}\right) & \omega t \in [0, \beta] \\ \frac{\sqrt{3}}{2}(0.5-k)\sin(\omega t) + \frac{1}{2}(1.5+k)\cos(\omega t) & \omega t \in [\beta, \frac{\pi}{6}] \\ \frac{\sqrt{3}}{2}(0.5+k)\sin(\omega t) + \frac{1}{2}(1.5-k)\cos(\omega t) & \omega t \in [\frac{\pi}{6}, \frac{\pi}{3} - \beta] \\ \frac{k+x+0.5}{x+1}\sin\left(\omega t + \frac{\pi}{6}\right) & \omega t \in [\frac{\pi}{3} - \beta, \frac{\pi}{3} + \beta] \\ \frac{\sqrt{3}}{2}\sin(\omega t) + k\cos(\omega t) & \omega t \in [\frac{\pi}{3} + \beta, \frac{\pi}{2}] \\ \frac{\sqrt{3}}{2}\sin(\omega t) - k\cos(\omega t) & \omega t \in [\frac{\pi}{2}, \frac{2\pi}{3} - \beta] \\ \frac{k+x+0.5}{x+1}\sin\left(\omega t - \frac{\pi}{6}\right) & \omega t \in [\frac{2\pi}{3} - \beta, \frac{2\pi}{3}]. \end{cases} \tag{47}$$

The rms value of the output voltage is determined as

$$V_L = \sqrt{3}V_m \times \sqrt{\frac{3}{2\pi}\left\{A_2 + A_3 k + A_4 k^2 + \frac{A_5(k+x+0.5)^2}{(x+1)^2}\right\}} \tag{48}$$

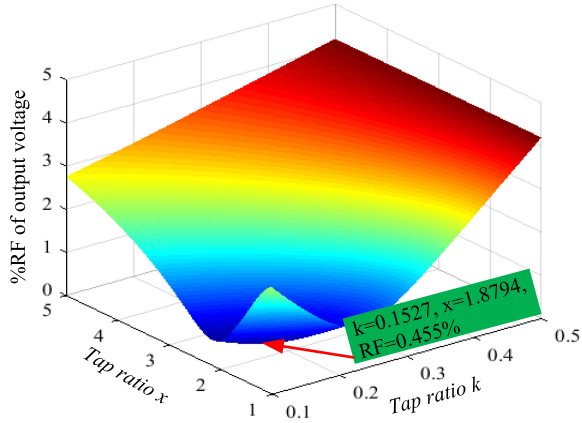

Fig. 7. Relation among RF, x, and k.

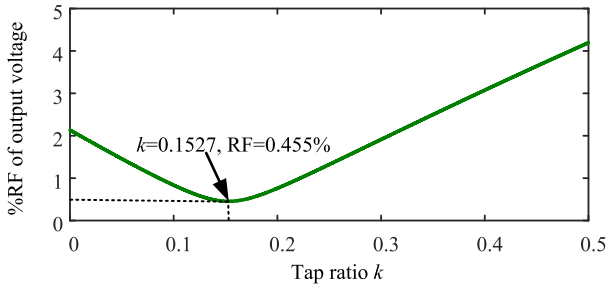

Fig. 8. Relation between RF and tap ratio k when $x = 1.8794$.

where

$$A_2 = \left[\frac{\pi}{4} - \frac{3\beta}{2} + \frac{3}{4}\sin\left(\frac{\pi}{3} - 2\beta\right)\right]$$

$$A_3 = \sqrt{3}\left[1 - \cos\left(\frac{\pi}{3} - 2\beta\right)\right]$$

$$A_4 = \left[\frac{\pi}{3} - 2\beta - \sin\left(\frac{\pi}{3} - 2\beta\right)\right], A_5 = \left[2\beta + \sin(2\beta)\right].$$

The average value of the output voltage is determined as

$$V_{L(a)} = \frac{6\sqrt{3}V_m}{\pi}\left[k + \frac{\sqrt{3}}{4}(1-2k)\cos\beta + A_6\sin\beta\right] \tag{49}$$

where $A_6 = (\frac{k+x+0.5}{x+1} - \frac{2k+3}{x+1})$.

Ripple factor (RF) of the output voltage is defined as

$$\%\mathrm{RF} = \frac{\sqrt{V_L^2 - V_{L(a)}^2}}{V_{L(a)}}. \tag{50}$$

RF of the output voltage is calculated by substituting (48) and (49) into (50). The relation among tap ratios k, x, and RF is shown in Fig. 7. Fig. 7 shows that RF of the output voltage is minimum when $k = 0.1527$ and $x = 1.8794$. Hence, optimum values of tap ratios k and x are 0.1527 and 1.8794, respectively, and under these optimum values, RF of the output voltage is about 0.455%. When $x = 1.8794$, the relation between RF and tap ratio k is shown in Fig. 8. When $k = 0.1527$, the relation between RF and tap ratio x is shown in Fig. 9.

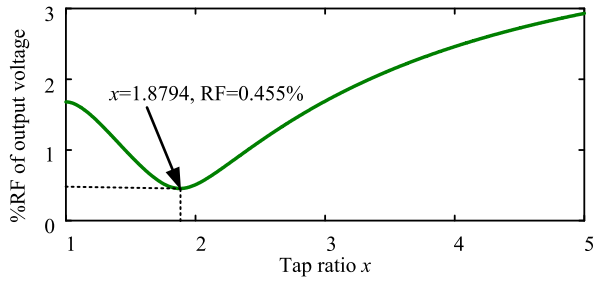

Fig. 9. Relation between RF and tap ratio x when $k = 0.1527$.

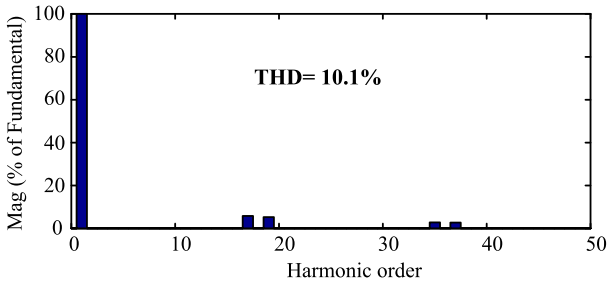

Fig. 10. Spectrum of input line current.

From the aforementioned analysis, it can be confirmed that the optimum values of tap ratios k and x are 0.1527 and 1.8794, respectively, and THD of the input line current and RF of the output voltage are minimum for these optimum values. Under optimum tap ratios, the proposed passive auxiliary circuits convert double-star rectifier to 18-pulse star rectifier. When $k = 0.1527$ and $x = 1.8794$, initial conduction angle β is determined from (40) and value of β is

$$\beta = \frac{\pi}{18}. \tag{51}$$

When $k = 0.1527$ and $x = 1.8794$, Fig. 10 shows the spectrum of the input line current. As shown in Fig. 10, THD of the input line current is about 10.1% and the proposed 18-pulse star rectifier eliminates lower than 17th-order harmonics.

V. Rating of Passive Auxiliary Circuit

A. Peak Reverse Voltage (PRV) Rating of Diode

Peak reverse voltage (PRV) rating of the diode D_x is determined in Y-mode because in this mode, reverse voltage across the diode D_x is maximum. For a similar reason, PRV rating of the diode D_y is determined in X-mode. PRV ratings of the diodes D_x and D_y are the same and expressed as

$$v_{Dx(\mathrm{PRV})} = v_{Dy(\mathrm{PRV})} = \frac{2x+1}{x+1}\sqrt{3}\,V_m. \tag{52}$$

PRV ratings of diodes D_r and D_s are determined in X-mode and Y-mode, respectively. PRV ratings of the diodes D_r and D_s are the same and expressed as

$$v_{Dr(\mathrm{PRV})} = v_{Ds(\mathrm{PRV})} = \frac{2k}{x+1}\sqrt{3}\,V_m. \tag{53}$$

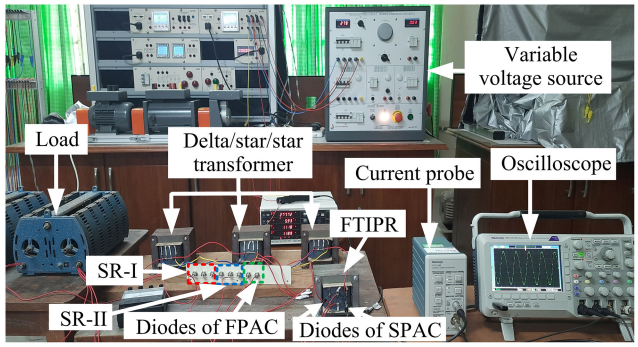

Fig. 11. Experimental setup for validating the proposed 18-pulse star rectifier.

TABLE I
Specifications of Experimental Prototype

Operation Parameter	Value
Input line to line voltage (rms)	280 V
Grid Frequency	50 Hz
Tap ratio k of the FTIPR	0.1527
Tap ratio x of the FTIPR	1.8794
Transformer turn ratio (Δ/Y/Y)	7:1:1
Magnetizing inductance of FTIPR	175 mH
Rated load current	10 A

B. Current Rating of Diode

From the analysis of operation mode, current through diode D_x is expressed as

$$i_x = \begin{cases} \frac{0.5-k}{x+1} I_L & \omega t \in [0 + \frac{2n\pi}{3}, \frac{\pi}{18} + \frac{2n\pi}{3}] \\ 0 & \omega t \in [\frac{\pi}{18} + \frac{2n\pi}{3}, \frac{11\pi}{18} + \frac{2n\pi}{3}] \\ \frac{0.5-k}{x+1} I_L & \omega t \in [\frac{11\pi}{18} + \frac{2n\pi}{3}, \frac{2\pi}{3} + \frac{2n\pi}{3}]. \end{cases} \tag{54}$$

Under optimum tap ratios, the maximum and rms values of the currents through diodes D_x and D_y are the same and calculated as

$$\begin{cases} i_{x(\max)} = i_{y(\max)} = 0.12062 I_L \\ I_x = I_y = 0.04924 I_L. \end{cases} \tag{55}$$

Furthermore, from the analysis of operation mode, current through diode D_r is expressed as

$$i_r = \begin{cases} 0 & \omega t \in [0 + \frac{2n\pi}{3}, \frac{\pi}{6} + \frac{2n\pi}{3}] \\ I_L & \omega t \in [\frac{\pi}{6} + \frac{2n\pi}{3}, \frac{\pi}{2} + \frac{2n\pi}{3}] \\ 0 & \omega t \in [\frac{\pi}{2} + \frac{2n\pi}{3}, \frac{2\pi}{3} + \frac{2n\pi}{3}]. \end{cases} \tag{56}$$

The maximum and rms values of the currents through diodes D_r and D_s are the same and calculated as

$$\begin{cases} i_{r(\max)} = i_{s(\max)} = I_L \\ I_r = I_s = 0.7071\, I_L. \end{cases} \tag{57}$$

C. KVA Rating of FTIPR

In this section, KVA rating of the FTIPR is determined under optimum tap ratios. The rms values of the currents for each winding of the FTIPR need to be determined. The currents through windings AB and EF are equal to currents i_y and i_x,

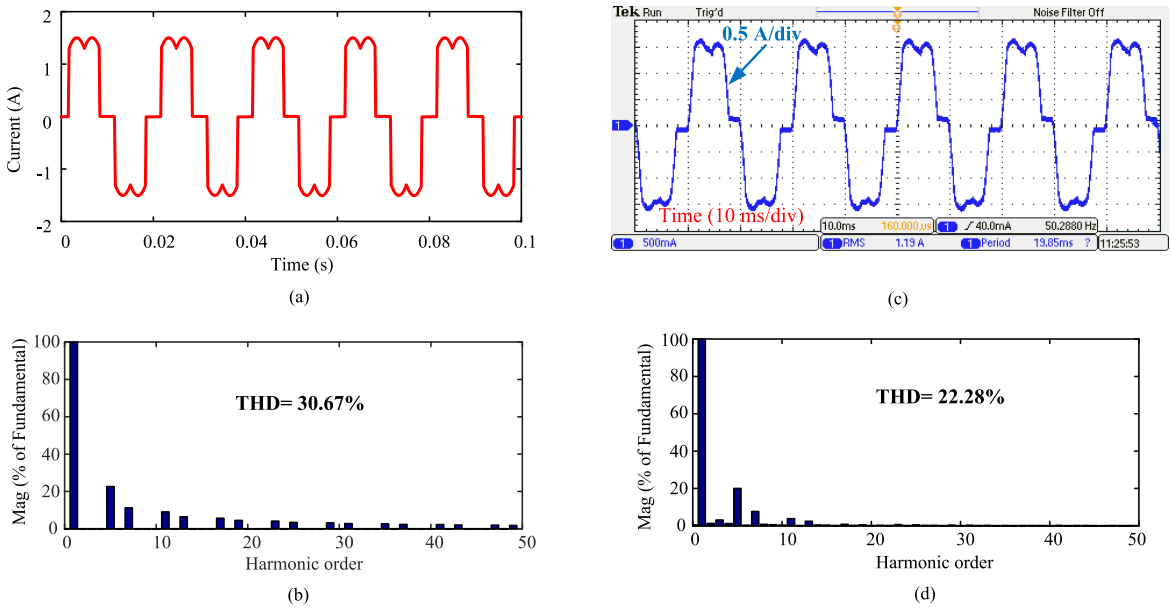

Fig. 12. (a) Input line current (simulation). (b) Spectrum of input line current (simulation). (c) Input line current (experimental). (d) Spectrum of input line current (experimental) of double-star six-pulse rectifier.

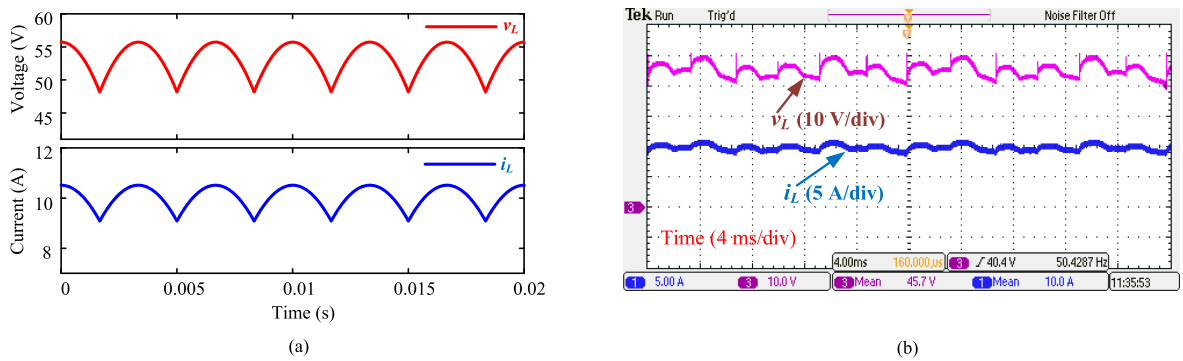

Fig. 13. Waveforms of output voltage and output current of double-star six-pulse rectifier. (a) Simulation. (b) Experimental.

respectively. The rms values of the currents through windings AB and EF are the same and calculated as

$$I_{\mathrm{AB}} = I_{\mathrm{EF}} = 0.04924 I_L. \tag{58}$$

From the analysis of operation mode, the rms values of the currents through windings BC and DE are the same and calculated as

$$I_{\mathrm{BC}} = I_{\mathrm{DE}} = 0.55993 I_L. \tag{59}$$

Furthermore, the rms value of the current through the winding CD is calculated as

$$I_{\mathrm{CD}} = 0.29199 I_L. \tag{60}$$

From (46) and (51), the rms value of the voltage v_n is calculated as

$$V_n = \sqrt{3}\, V_m \times 0.25734. \tag{61}$$

Furthermore, from (49) and (51), the average value of the output voltage is calculated as

$$V_{L(a)} = \sqrt{3}\, V_m \times 0.87493. \tag{62}$$

Therefore, KVA rating of the FTIPR is calculated as

$$\begin{aligned} S_{\mathrm{FTIPR}} &= \frac{1}{2}\{xV_nI_{\mathrm{AB}} + (0.5-k)V_nI_{\mathrm{BC}} + 2kV_nI_{\mathrm{CD}} \\ &\quad + (0.5-k)V_nI_{\mathrm{DE}} + xV_nI_{\mathrm{EF}}\} \\ &= \sqrt{3}\, V_m i_L \times 0.08533 \\ &= 9.75\%\, V_{L(a)} I_L. \end{aligned} \tag{63}$$

In the proposed 18-pulse star rectifier, KVA rating of the FTIPR is 9.75% of the load power.

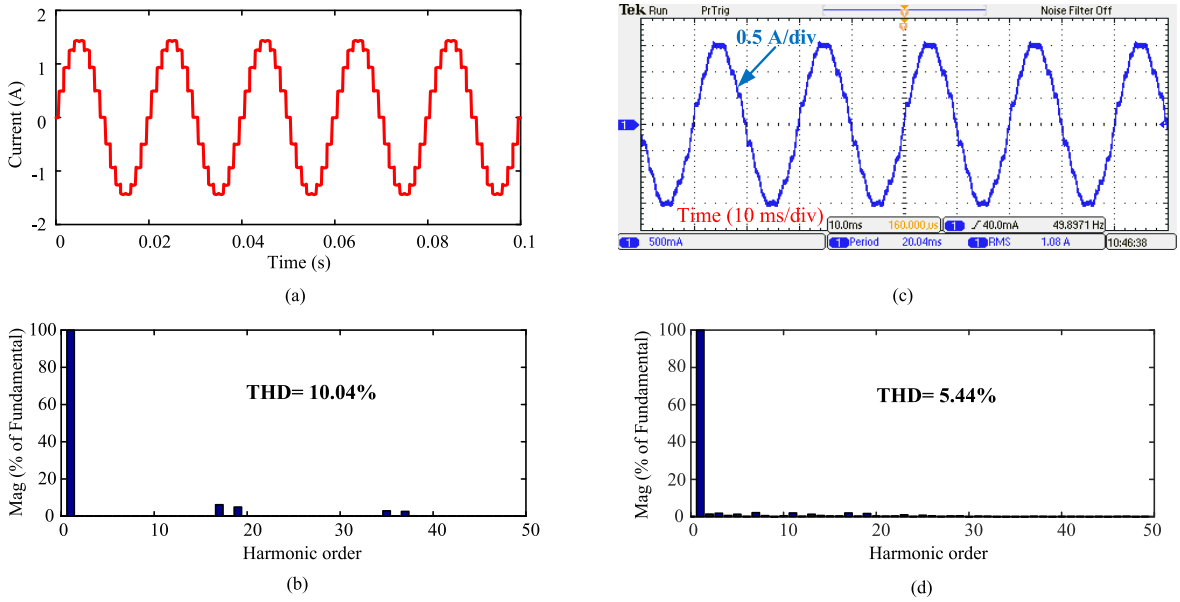

Fig. 14. (a) Input line current (simulation). (b) Spectrum of input line current (simulation). (c) Input line current (experimental). (d) Spectrum of input line current (experimental) of the proposed 18-pulse star rectifier.

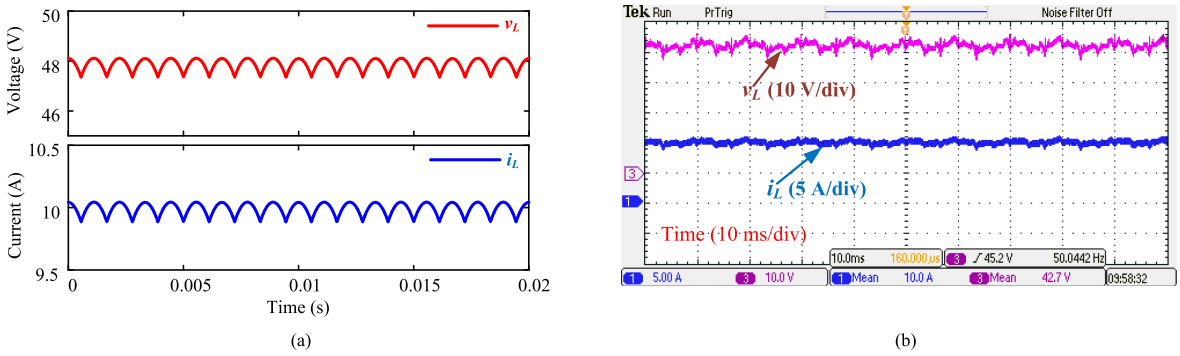

Fig. 15. Waveforms of output voltage and output current of the proposed 18-pulse star rectifier. (a) Simulation. (b) Experimental.

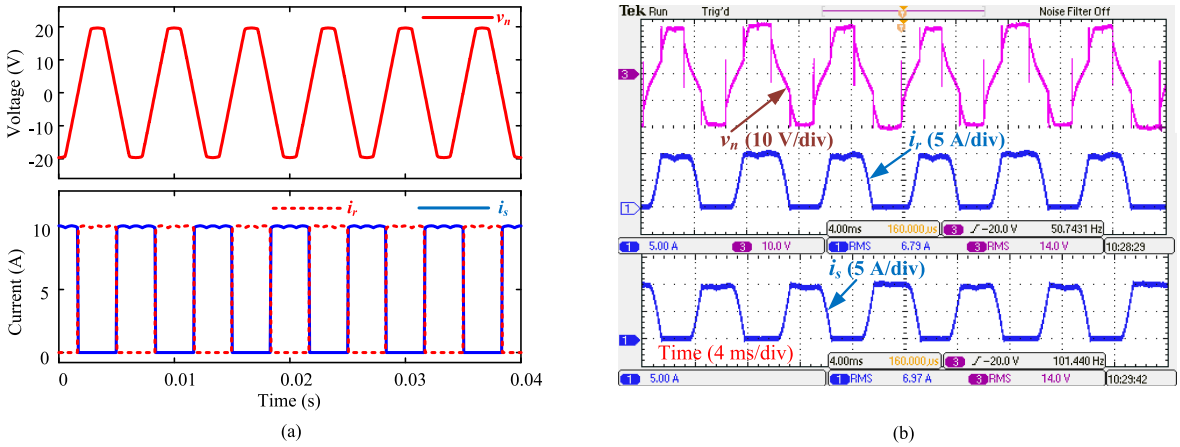

Fig. 16. Waveforms of voltage v_n, current i_r, and current i_s. (a) Simulation. (b) Experimental.

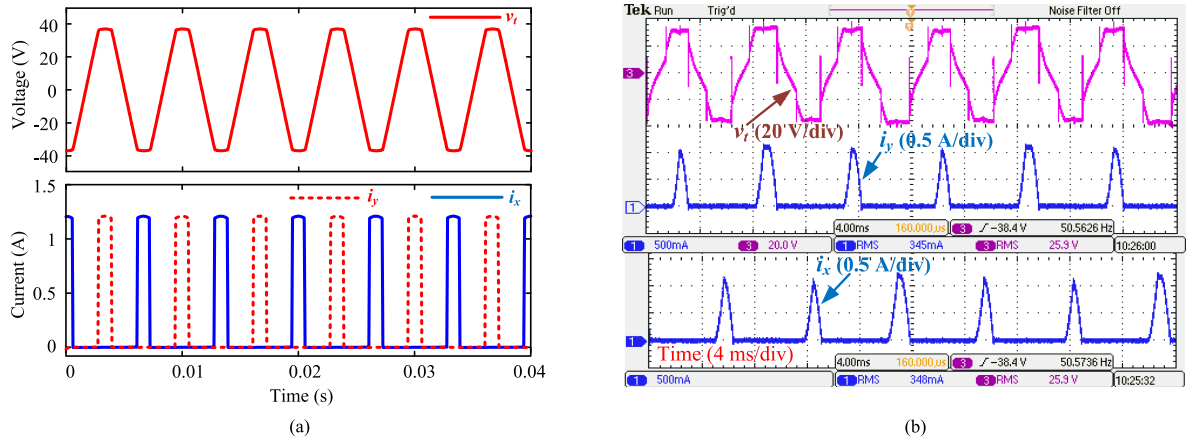

Fig. 17. Waveforms of voltage v_t, current i_y, and current i_x. (a) Simulation. (b) Experimental.

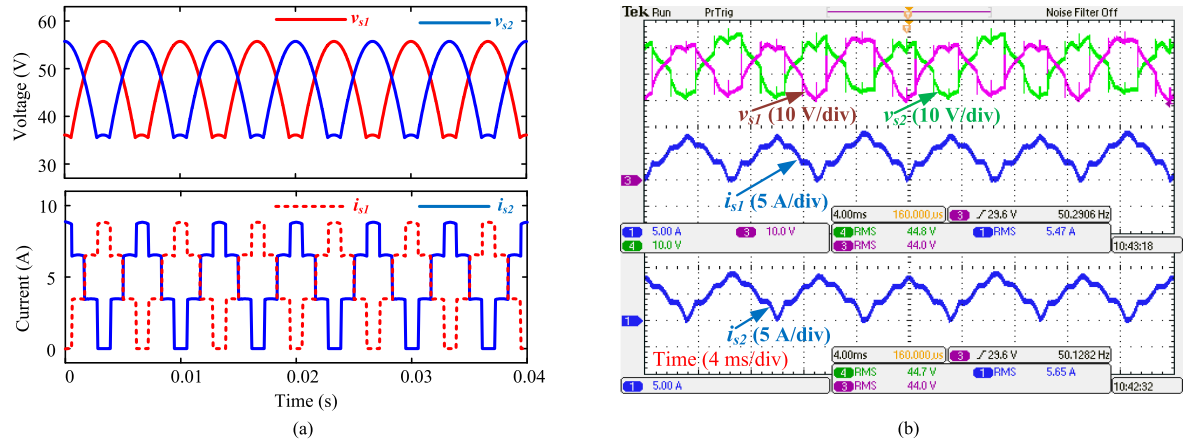

Fig. 18. Waveforms of voltage v_{s1}, voltage v_{s2}, current i_{s1}, and current i_{s2}. (a) Simulation. (b) Experimental.

VI. Simulation and Experimental Result

Simulation and experimental results are presented in this section to verify the overall performance of the proposed 18-pulse star rectifier. Photograph of the experimental prototype is shown in Fig. 11 and specifications of the experimental prototype are given in Table I. Simulation is carried out in the MATLAB/Simulink, and specifications in Table I are also considered in the simulation.

When FPAC and SPAC are not used in the proposed rectifier scheme, the proposed rectifier operates as double-star six-pulse rectifier. Fig. 12(a) and (b) shows the simulation waveforms of the input line current and its spectrum of the double-star rectifier, respectively, and Fig. 12(c) and (d) shows the corresponding experimental waveform of the input line current and its spectrum, respectively. Simulation and experimental values of THD are 30.67% and 22.28%, respectively, and fifth harmonics is the lowest order harmonics. Experimental value of THD is lower than the simulation value of THD due to leakage inductance of the delta/star/star transformer.

Simulation and experimental waveforms of the output voltage and output current of the double-star rectifier are shown in Fig. 13(a) and (b), respectively. Output voltage and output current of the double-star rectifier contain six pulses per cycle. Because of the unbalance in the grid voltage and slight asymmetry in the experimental setup, magnitude of each pulse is not the same in the experimental result. Resistor is used as a load, and 5.3 and 4.57 Ω resistance of the load are considered in simulation and experiment, respectively, to limit the 10-A load current.

When FPAC and SPAC are used, the proposed rectifier operates as 18-pulse star rectifier. Fig. 14(a) and (b) shows the simulation waveforms of the input line current and its spectrum of the proposed 18-pulse star rectifier, respectively. As shown in Fig. 14(b), THD of the input line current in simulation is 10.04% and the lowest harmonic is 17th order. Fig. 14(c) and (d) shows the experimental waveforms of the input line current and its spectrum of the proposed 18-pulse star rectifier, respectively, showing THD of the input line current as 5.44%, which is less than the simulation value of 10.04% due to leakage inductance of the delta/star/star transformer. The experimental input line current contains small amount of fifth- and seventh-order harmonics due to unbalance in the grid voltages and slight asymmetry in the experimental setup. Compared with the double-star rectifier, the proposed passive auxiliary circuits have strong harmonics suppression ability.

Simulation waveforms of the output voltage and output current of the proposed 18-pulse star rectifier are shown in Fig. 15(a), which contain 18 pulses per cycle. Experimental waveforms of the output voltage and output current of the proposed 18-pulse star rectifier are shown in Fig. 15(b). Output voltage and output current are smoothed due to leakage inductance of the delta/star/star transformer; therefore, 18 pulses per cycle cannot be identified in experimental results. Resistor is used as a load, and 4.79 and 4.27 Ω resistance of the load are considered in simulation and experiment, respectively, to limit the 10-A load current.

Fig. 16(a) shows the simulation waveforms of the voltage v_n of the FTIPR, and the currents i_r and i_s of the FPAC; and Fig. 16(b) shows the corresponding experimental results. Frequency of the trapezoidal shaped voltage v_n is three times of the grid frequency. Diodes D_r and D_s are alternately turned ON three times per cycle.

Fig. 17(a) shows simulation waveforms of the voltage v_t of the FTIPR, and the currents i_y and i_x of the SPAC; and corresponding experimental results are shown in Fig. 17(b). Frequency of the trapezoidal shaped voltage v_t is three times of the grid frequency and magnitude is 1.8794 times of the voltage v_n. Diodes D_y and D_x are turned ON three times per cycle.

Fig. 18(a) shows the simulation waveforms of the output voltages and output currents of SR-I and SR-II; and Fig. 18(b) shows the corresponding experimental results. The state of the output voltages and output currents of SR-I and SR-II is increased due to the operation of the FPAC and SPAC. The changes in the voltages and currents of SR-I and SR-II upgrade double-star rectifier to 18-pulse star rectifier. The waveforms of Fig. 18 are consistent with the theoretical waveforms, which are shown in Fig. 3(g)–(j).

VII. Conclusion

Two passive auxiliary circuits are proposed for double-star rectifier to achieve 18-pulse star rectifier operation. FPAC and SPAC need FTIPR along with four additional diodes. FPAC and SPAC increase the state of the output voltages and output currents of SR-I and SR-II, which upgrade double-star rectifier into 18-pulse star rectifier. Tap ratios of the FTIPR are optimally designed from the viewpoint of minimum THD of the input line current and minimum ripple of the output voltage. Under optimum tap ratios, output voltage of the proposed rectifier contains 18 pulses per cycle and input line current contains 18 steps per cycle. After using the FPAC and SPAC in double-star rectifier, experimental THD of the input line current reduces from 22.28% to 5.44%. The existing double-star rectifier can be easily converted into proposed 18-pulse star rectifier without much modification within the existing system design. Since only four diodes and FTIPR are used in FPAC and SPAC, the proposed rectifier is completely passive.

Acknowledgment

The authors would like to thank Dr. Md. Samiul Habib for fruitful discussion.

References

[1] A. Siebert, A. Troedson, and S. Ebner, "AC to DC power conversion now and in the future," *IEEE Trans. Ind. Appl.*, vol. 38, no. 4, pp. 934–940, Jul./Aug. 2002.

[2] *IEEE Recommended Practices and Requirements for Harmonic Control in Electrical Power Systems*, IEEE Standard-519, 1992.

[3] P. P. S., R. Kalpana, B. Singh, and G. Bhuvaneswari, "A 20-pulse asymmetric multi-phase staggering autoconfigured transformer for power quality improvement," *IEEE Trans. Power Electron.*, vol. 33, no. 2, pp. 917–925, Feb. 2018.

[4] G. Olivier, G. E. April, E. Ngandui, and C. Guimaraes, "Novel transformer connection to improve current sharing in high-current DC rectifiers," *IEEE Trans. Ind. Appl.*, vol. 31, no. 1, pp. 127–133, Jan./Feb. 1995.

[5] B. Singh and S. Gairola, "Zigzag autotransformer based full-wave AC–DC converters," *Asian Power Electron. J.*, vol. 2, no. 1, pp. 23–30, Apr. 2008.

[6] F. Meng, P. Liu, L. Gao, Y. Yang, and S. Yang, "Optimal design of star-connected autotransformer applied to large current rectifier," *IET Electr. Power Appl.*, vol. 11, no. 1, pp. 80–89, Jan. 2017.

[7] M. A. Malek, M. A. G. Khan, and M. M. Islam, "An 18-pulse uncontrolled star rectifier for input line current harmonic reduction," in *Proc. 3rd Int. Conf. Elect. Comput. Telecommun. Eng.*, Rajshahi, Bangladesh, 2019, pp. 240–243.

[8] F. Meng, X. Xu, L. Gao, and C. Cai, "Active harmonic reduction using dc-side current injection applied in a novel large current rectifier based on fork-connected autotransformer," *IEEE Trans. Ind. Electron.*, vol. 64, no. 7, pp. 5250–5264, Jul. 2017.

[9] S. Miyairi, S. Iida, K. Nakata, and S. Masukawa, "New method for reducing harmonics involved in input and output of rectifier with interphase transformer," *IEEE Trans. Ind. Appl.*, vol. IA-22, no. 5, pp. 790–797, Sep. 1986.

[10] J. Wang, X. Yao, Q. Guan, and S. Yang, "A novel 12-pulse full-wave rectifier with simple circuit configuration," *Int. J. Circ. Theor. Appl.*, vol. 48, no. 10, pp. 1676–1695, Oct. 2020.

[11] M. A. Malek and M. A. G. Khan, "A new 36-pulse star rectifier for power quality improvement," in *Proc. 5th Int. Conf. Adv. Elect. Eng.*, Dhaka, Bangladesh, 2019, pp. 102–107.

[12] J. Wang, X. Yao, X. Gao, and S. Yang, "Harmonic reduction for 12-pulse rectifier using two auxiliary single-phase full-wave rectifiers," *IEEE Trans. Power Electron.*, vol. 35, no. 12, pp. 12617–12622, Dec. 2020.

[13] F. Meng, X. Xu, L. Gao, Z. Man, and X. Cai, "Dual passive harmonic reduction at dc link of the double-star uncontrolled rectifier," *IEEE Trans. Ind. Electron.*, vol. 66, no. 4, pp. 3303–3309, Apr. 2019.

[14] Y. Lian, S. Yang, X. Zeng, H. Ben, and W. Yang, "Comparative analysis of two different interphase reactors applied in 36-pulse diode rectifier," *IET Electr. Power Appl.*, vol. 14, no. 6, pp. 1011–1022, Jun. 2020.

Md. Abdul Malek (Graduate Student Member, IEEE) received the B.Sc. and M.Sc. degrees in electrical & electronic engineering from the Rajshahi University of Engineering & Technology (RUET), Rajshahi, Bangladesh, in 2017 and 2021, respectively.

Since 2019, he has been a Lecturer with the Department of Electrical & Electronic Engineering, RUET. His research interests include power electronics and power quality improvement.

Muhammad Abdul Goffar Khan (Senior Member, IEEE) received the B.Sc. degree in electrical & electronic engineering (EEE) from the Rajshahi University of Engineering & Technology (RUET), in 1983, the M.Sc. degree in EEE from the Bangladesh University of Engineering and Technology (BUET), in 1987, and the Ph.D. degree in high voltage engineering from the Indian Institute of Technology, Kanpur (IITK), Kanpur, India, in 1997.

Since 2002, he has been a Professor with RUET. He has authored or coauthored more than 80 research papers in different journals and conference proceedings. His research interests include power electronics, high-voltage engineering, renewable energy, advanced optical fibers, etc.

Dr. Khan is an active member of different professional organizations. He was the elected Vice Chair of IEEE Bangladesh section for three consecutive years of 2015, 2016, and 2017.